available at www.sciencedirect.com

ScienceDirect

journal homepage: www.elsevier.com/locate/jmbbm

Research paper

Structure and mechanical properties of *Saxidomus purpuratus* biological shells

W. Yang[a,b], G.P. Zhang[a,*], X.F. Zhu[a], X.W. Li[b], M.A. Meyers[c,d]

[a] *Shenyang National Laboratory for Materials Science, Institute of Metal Research, Chinese Academy of Sciences, 72 Wenhua Road, Shenyang 110016, PR China*
[b] *Institute of Materials Physics and Chemistry, College of Sciences, Northeastern University, Shenyang 110004, PR China*
[c] *Department of Mechanical and Aerospace Engineering, University of California, San Diego, La Jolla, CA 92093-0411, USA*
[d] *Department of Nanoengineering, University of California, San Diego, La Jolla, CA 92093-0411, USA*

ARTICLE INFO

Article history:
Received 26 October 2010
Received in revised form
6 May 2011
Accepted 7 May 2011
Published online 17 May 2011

Keywords:
Shell
Strength
Fracture
Microstructure
Bending
Compression
Bivalves
Saxidomus purpuratus

ABSTRACT

The strength and fracture behavior of *Saxidomus purpuratus* shells were investigated and correlated with the structure. The shells show a crossed lamellar structure in the inner and middle layers and a fibrous/blocky and porous structure composed of nanoscaled particulates (~100 nm diameter) in the outer layer. It was found that the flexure strength and fracture mode are a function of lamellar organization and orientation. The crossed lamellar structure of this shell is composed of domains of parallel lamellae with approximate thickness of 200–600 nm. These domains have approximate lateral dimensions of 10–70 μm with a minimum of two orientations of lamellae in the inner and middle layers. Neighboring domains are oriented at specific angles and thus the structure forms a crossed lamellar pattern. The microhardness across the thickness was lower in the outer layer because of the porosity and the absence of lamellae. The tensile (from flexure tests) and compressive strengths were analyzed by means of Weibull statistics. The mean tensile (flexure) strength at probability of 50%, 80–105 MPa, is on the same order as the compressive strength (~50–150 MPa) and the Weibull moduli vary from 3.0 to 7.6. These values are significantly lower than abalone nacre, in spite of having the same aragonite structure. The lower strength can be attributed to a smaller fraction of the organic interlayer. The fracture path in the specimens is dominated by the orientation of the domains and proceeds preferentially along lamella boundaries. It also correlates with the color changes in the cross section of the shell. The cracks tend to undergo a considerable change in orientation when the color changes abruptly. The distributions of strengths, cracking paths, and fracture surfaces indicate that the mechanical properties of the shell are anisotropic with a hierarchical nature.

* *Corresponding author.* Tel.: +86 24 23971938; fax: +86 24 23891320.
E-mail address: gpzhang@imr.ac.cn (G.P. Zhang).

1751-6161/$ - see front matter © 2011 Elsevier Ltd. All rights reserved.
doi:10.1016/j.jmbbm.2011.05.021

1. Introduction

Mollusk shells are natural multilayered composite structures that usually exhibit excellent mechanical properties due to the hierarchical organization of calcium carbonate layers and organic interlayers. Whereas the mineral is hard as well as brittle and the organic layer is soft, their combination provides excellent toughness. Because of these outstanding properties, there have been numerous studies correlating the mechanical properties and structure of shells. Extensive investigations have been conducted on the structures and mechanical behavior of different classes of shells: the gastropods abalone (Nakahara et al., 1982; Sarikaya et al., 1990; Sarikaya and Aksay, 1992; Zaremba et al., 1996; Menig et al., 2000; Su et al., 2002; Song et al., 2003; Lin and Meyers, 2005; Nukala and Simunovic, 2005; Li et al., 2006; Lin et al., 2006, 2008; Meyers et al., 2008) and conch (Currey and Kohn, 1976; Currey, 1977; Laraia and Heuer, 1989; Kuhn-Spearing et al., 1996; Menig et al., 2001; Su et al., 2004); the bivalves clam (Taylor and Layman, 1972; Checa and Rodríguez-Navarro, 2005; Kobayashi and Samata, 2006; Lin et al., 2006) and oyster (Currey, 1977; Checa and Rodríguez-Navarro, 2005; Checa et al., 2005; Kobayashi and Samata, 2006), for instance.

To some extent, the nacreous structure of shells has the highest mechanical properties; it is composed of parallel layers of lamellae. In the *Strombus gigas* (conch), the good mechanical properties are attributed to the crossed lamellar structure, which inhibits crack propagation and delocalizes damage (Currey and Kohn, 1976). As a result, the crack has to travel along the intertile layers creating a tortuous path, and accordingly the toughness and the work of fracture are enhanced. The complex structure and anisotropy of the shells caused by the growth process lead to positional and orientational dependences of the mechanical properties. There have been significant recent efforts to computationally model the mechanical behavior of the shells, especially the interface features (Evans et al., 2001; Katti et al., 2001; Gao et al., 2003; Nukala and Simunovic, 2005; Barthelat et al., 2006; Katti and Katti, 2006; Barthelat et al., 2007; Tang et al., 2007; Ji, 2008).

Bending and compression results obtained by a number of investigators for a large number of shells are summarized in Tables 1 and 2, respectively. The reported three/four-point bending strengths vary from 4.1 MPa (Taylor and Layman, 1972) (foliated structure of *Crassostrea gigas*) to 370 MPa (Wang et al., 2001) (nacre structure of *Haliotis rufescens*). It is clear that there is a great variation in the strengths. Some of the differences listed are due to the differences in testing procedures between investigators. Some of the reported results were wrong and are corrected in Tables 1 and 2 by the present authors. For example, in one paper (Taylor and Layman, 1972), the wrong unit of modulus was given so that their results were three orders of magnitude lower; according to the data shown in paper, some of the moduli of the shells, such as *C. gigas*, were calculated incorrectly. From these results summarized in Tables 1 and 2, we can conclude that the strengths of the shells are not distinguished by their classes. Some shells with the crossed lamellar structure can exhibit a higher strength than the nacreous structure. The largest flexure strengths reported are 370 MPa for *H. rufescens* (Wang et al., 2001) and 360 MPa for *Pinctada maxima* (Taylor and Layman, 1972). The maximum compressive strengths in quasi-static tests are 540 MPa for *H. rufescens* (Menig et al., 2000, loading perpendicular to lamellae) and 567 MPa for Araguaia river clam (Chen et al., 2008, loading perpendicular to lamellae). In general, the strengths of the wet specimens are lower than the strengths of the dry ones, although the toughness of the wet shells is higher.

The goal of this research was to elucidate strength and fracture mechanisms in the *Saxidomus purpuratus* shells by means of systematic examination of microstructures, bending strength, microhardness and fracture behavior of the shells. Particular attention is devoted to the orientational and positional dependences of the mechanical properties and their relationship to the structure. A thorough comparison between the present results and those reported in literature is also conducted. Although abalone and conch have been the subjects of numerous investigations, the *Saxidomus* shell has not had its structure correlated with mechanical properties. The other study, to our acknowledge, is by Jia et al. (2006) who focused on the structure and friction-wear characteristics.

2. Experimental methods

Shells of *S. purpuratus*, belonging to the mollusk class Bivalvia were taken from the Huang/Bo sea area of China. To obtain complete shells, the inside soft tissue was removed carefully; they were subsequently cleaned with deionized water. The lengths of the shells were typically around 100 mm and their heights about 75 mm. Representative shells are shown in Fig. 1. The growth starts at the top of the dorsal part (top portion) and proceeds down. Two growth lines marked in Fig. 1(a) indicate the edges of shell at different stages of growth.

Fig. 1(a) shows the positions of a number of specimens for three-point bending tests cut parallel. It can be seen that they make varying angles with the growth lines. The final dimensions of the specimens were $22.8 \times 4.0 \times 1.2$ mm^3.

A limited number of compression tests were conducted to investigate the relationship between cracking paths and compression curves. More detailed measurements are reported by Yang et al. (2011a). Fig. 1(b) shows the positions of a number of compression test specimens. The parallelepiped in the figure represents the compression specimens. The approximate dimensions are $2 \times 2 \times 4$ mm^3. All specimens were carefully ground with emery papers from 400# to 2000#.

The three-point bending and compression tests were conducted under constant loading rates of 1 μm/s and 0.5 μm/s, respectively, with an Instron E1000 machine. The bending loading direction was from the outer layer to inner layer. Thus, the inner layer is subjected to tensile stress. The bending strength was calculated using the common flexure equation (e. g. Meyers and Chawla, 1999). The loading span for the bending test was 20 mm; approximately fifteen specimens were tested for a single shell. To obtain statistical results, four dry valves and two wet valves were tested in three-point bending. Microindentation tests were performed on the cross section of the shell from inner to the outer layer to obtain the hardness of the specimen.

Table 1 – Bending strengths of different shells obtained from the literature.

Class	Name	Structure	Test direction	Condition	σ (MPa)	E (GPa)	Reference
Bivalves		SN	Parallel		37.8	44.0	Currey and Taylor, 1974
	Anodonta cygnea	SN		Wet*	35 ± 2.5		Currey, 1977
		SN			117 ± 9.8	44 ± 1.5	Currey, 1976
	Araguaia river clam		Perpendicular		18.9[W]		Chen et al., 2008
			Parallel		17.9[W]		Chen et al., 2008
				Dry	107.6	31.1$^{\nabla}$	Taylor and Layman, 1972
	Arctica islandica			Wet	143.5	44.6$^{\nabla}$	Taylor and Layman, 1972
		H			60 ± 6.9	60 ± 5.8	Currey, 1976
		CP	Normal		60	39.2	Currey and Taylor, 1974
		SN	Normal		89.1	57.7	Currey and Taylor, 1974
	Atrina vexillum	SN		Wet*	86 ± 10.2		Currey, 1977
		SN			173 ± 23.6	58	Currey, 1976
		P			139 ± 14.1	39 ± 6.5	Currey, 1976
	Chama lazarus	CCL	Parallel			82.2	Currey and Taylor, 1974
		CCL			36 ± 2.4	82	Currey, 1976
	Crassostrea gigas	F		Wet	4.1	2.9$^{\nabla}$	Taylor and Layman, 1972
	Egeria radiata	FCL	Parallel		50.2	76.8	Currey and Taylor, 1974
	Egeria sp.	CL			106 ± 20.6	77 ± 1.4	Currey, 1976
	Ensis siliqua	FCL	Parallel			54.9	Currey and Taylor, 1974
		CL			85 ± 13.9	55	Currey, 1976
	Hippopus hippopus	CL	Normal		9.3	53.3	Currey and Taylor, 1974
		CL			35 ± 2.3	50 ± 2.8	Currey, 1976
		CN	Parallel		71.8	67.1	Currey and Taylor, 1974
	Hyria ligatus	SN			211 ± 20.7	44 ± 6.2	Currey, 1976
		SN		Wet*	79 ± 5		Currey, 1977
	Mercenaria mercenaria	FCL to H	Parallel		31.5	65.9	Currey and Taylor, 1974
		CL			95 ± 12.3	66	Currey, 1976
		SN		Wet*	56 ± 13.4		Currey, 1977
	Modiolus modiolus	SN		Wet	213	31.8$^{\nabla}$	Taylor and Layman, 1972
				Dry	238	47.6$^{\nabla}$	Taylor and Layman, 1972
		SN			199 ± 7.4	31 ± 2.4	Currey, 1976
	Ostrea edulis	F				47	Currey and Taylor, 1974
		F			93 ± 9.6	34 ± 1.8	Currey, 1976
	Pecten maximus	F	Normal		42.1	30.1	Currey and Taylor, 1974
		F			110 ± 8.2	30 ± 3.2	Currey, 1976
		SN	45°		51.1	48.4	Currey and Taylor, 1974
	Pinctada		Across	Dry		73 ± 9	Jackson et al., 1988
			Across	Wet		64 ± 8	Jackson et al., 1988
			Along	Dry		70 ± 11	Jackson et al., 1988
			Along	Wet		60 ± 10	Jackson et al., 1988
	Pinctada sp.	S		Wet*	56 ± 4.7		Currey, 1977
		SN			180 ± 5.8	48	Currey, 1976
	Pinctada margaritifera	SN			208±12.6	34 ± 3.1	Currey, 1976
		S		Wet*	87 ± 7.6		Currey and Kohn, 1976; Currey, 1977
			Long specimens	Wet*	106 ± 4.6		Currey and Kohn, 1976; Currey, 1977
		CP		Dry	99.4	19.9$^{\nabla}$	Taylor and Layman, 1972
		SN		Dry	360.8	46.9$^{\nabla}$	Taylor and Layman, 1972
	Pinctada maxima		Tensile(four)		140		Wang et al., 2001
			Compressive(four)		350$^{\otimes}$		Wang et al., 2001
			Parallel		248 ± 14	81 ± 4	Wang et al., 2001
			Perpendicular		227 ± 13	77 ± 12	Wang et al., 2001
	Pinna muricata	CP	Normal		62.4	11.8	Currey and Taylor, 1974
		P				12	Currey, 1976
	Saccostrea cucullata	F	Normal		31.2	28.7	Currey and Taylor, 1974
		CoF			44 ± 7.6	29 ± 3.9	Currey, 1976

Table 1 (*continued*)

Class	Name	Structure	Test direction	Condition	σ (MPa)	E (GPa)	Reference
	Saxidomus purpuratus	CL	Parallel	Dry	98 [W]		Present work
				Wet	91 [W]		Present work
	Tridacna gigas		Parallel(outer)		39.9		Lin et al., 2006
			Perpendicular(outer)		79.6		Lin et al., 2006
	Tridacna maxima	CCL		Dry	87. 1	25.6^{∇}	Taylor and Layman, 1972
				Wet	75	19.2^{∇}	Taylor and Layman, 1972
		CL		Dry	117. 9	32.0^{∇}	Taylor and Layman, 1972
				Wet	85	21.3^{∇}	Taylor and Layman, 1972
	Conus betulina Linnaeus	CL	Plane		31.76		Liang et al., 2008
			Transverse		22.14		Liang et al., 2008
	Conus leopardus	CL			130 ± 27.4	56 ± 4.6	Currey, 1976
	Conus miles	CL			63 ± 5.6	30 ± 2.0	Currey, 1976
	Conus litteratus	CL			80 ± 4.6		Currey, 1976
	Conus prometheus	CL	Parallel		34.9	67.7	Currey and Taylor, 1974
		CL			134 ± 17.5	58 ± 6.8	Currey, 1976
	Conus striatus	CL			108 ± 6.7		Currey, 1976
					70–200		Currey and Kohn, 1976
	Conus virgo	CL			165 ± 5.4		Currey, 1976
	Cypraea tigris	CL			156 ± 16.9	41 ± 3.6	Currey, 1976
	Haliotis rufescens	N	Parallel		177		Menig et al., 2000
			Perpendicular		197		Menig et al., 2000;
			Parallel		194 ± 8	66 ± 2	Wang et al., 2001
			Perpendicular		223 ± 7	69 ± 7	Wang et al., 2001
			Tensile(four)		105		Wang et al., 2001
			Compressive(four)		370	70	Wang et al., 2001
	Lambis lambis	CL			66 ± 15.1	39 ± 4.8	Currey, 1976
	Patella mexicana	CF	Parallel		33.2	60	Currey and Taylor, 1974
		CF			171 ± 18.0	60 ± 1.4	Currey, 1976
	Patella vulgata	CF			39 ± 5.6	18 ± 3.2	Currey, 1976
	Strombus costatus	CL			58 ± 6.5	49 ± 2.4	Currey, 1976
	Strombus gigas	CL	Parallel			48.6	Currey and Taylor, 1974
			Four		100		Menig et al., 2001; Laraia and Heuer, 1989
Gastropods			Four	Dry	182 ± 71		Kuhn-Spearing et al., 1996
			Four	Wet	215 ± 71		Kuhn-Spearing et al., 1996
			Four (without inner layers)	Dry	56 ± 22		Kuhn-Spearing et al., 1996
			Four (without inner layers)	Wet	84 ± 49		Kuhn-Spearing et al., 1996
		CL	Parallel		6.2	40.7	Currey and Taylor, 1974
		CL			78 ± 15.7	41 ± 3.5	Currey, 1976
			Perpendicular		29		Lin et al., 2006
			Parallel		74		Lin et al., 2006
			Parallel		52–74		Menig et al., 2001
			Perpendicular		24–29		Menig et al., 2001
	Trochus niloticus	CN		Wet*	85 ± 3.5		Currey, 1977
		CN			220 ± 3.8	64 ± 1.6	Currey, 1976
		CN		Wet*	116 ± 14.5		Currey, 1977
	Turbo marmoratus	CN	Normal		107.8	54.1	Currey and Taylor, 1974
		N			63.1	44.5	Currey and Taylor, 1974
		CN			267 ± 10.2	54 ± 5.8	Currey, 1976

S: sheet, N: nacre, SN: sheet nacre, H: homogeneous, CP: calcite prisms, CL: cross-lamellar, CCL: complex cross-lamellar, F: foliated, FCL: fine cross-lamellar, CF: cross-foliated, CN: columnar nacre, CoF: complex foliated.
Data with $^{\nabla}$ are corrected values. ⊗ are measured from references by authors. Specimens with the condition of wet* have been dried out at some stage but were machined and tested wet. σ: bending strength; E: modulus [W] means data are obtained with Weibull method.

Fracture surfaces of the specimens were examined in LEO Supra 35 and FEI scanning electron microscopes (SEM) as well as Phillips XL 30 environmental scanning electron microscopy (ESEM). Before observation, fracture surfaces were sputtered

Table 2 – Compression strengths of different shells obtained from the literature.

Class	Name	Structure	Test orientation	Treatment	Strength (MPa)	E (GPa)	Note	Reference
Bivalve	*Anodonta cygnea*	SN			322±47.8			Currey, 1976
	Araguaia river clam	N	Parallel		347		W	Chen et al., 2008
			Perpendicular		567		W	Chen et al., 2008
	Arctica islandica	H		Wet	324±40	6.5$^{\nabla}$		Taylor and Layman, 1972
				Dry	374±50	8.7$^{\nabla}$		Taylor and Layman, 1972
		H			248±17.3			Currey, 1976
	Atrina vexillum	SN			304±31.1			Currey, 1976
		P			295±25.1			Currey, 1976
	Chama lazarus	CCL			222±34.9			Currey, 1976
	Codakia tigerina	CMP		Dry	108±10	6.0$^{\nabla}$		Taylor and Layman, 1972
	Egeria sp.	CL			163±12.4			Currey, 1976
	Ensis siliqua	CL			196±40.1			Currey, 1976
	Glycymeris glycymeris	CL		Wet	83.3±10	6.9$^{\nabla}$		Taylor and Layman, 1972
				Dry	132±40	8.8$^{\nabla}$		Taylor and Layman, 1972
	Hippopus hippopus	CL			229±40.0			Currey, 1976
	Hyria ligatus	SN			382±36.9			Currey, 1976
	Mercenaria mercenaria	CMP/H		Wet	315±50	9.0$^{\nabla}$		Taylor and Layman, 1972
				Dry	238±40	9.9		Taylor and Layman, 1972
		CL			336±37.4			Currey, 1976
	Modiolus modiolus	SN		Wet	334±60	6.7$^{\nabla}$		Taylor and Layman, 1972
				Dry	393±40	7.9$^{\nabla}$		Taylor and Layman, 1972
		SN			416±48.2			Currey, 1976
	Neotrigonia margaritacea	LN		Dry	306	8.5$^{\nabla}$		Taylor and Layman, 1972
	Ostrea edulis	F			82±12.1			Currey, 1976
	Pecten maximus	F		Wet	102	4.9		Taylor and Layman, 1972
				Dry	203±40	7.0$^{\nabla}$		Taylor and Layman, 1972
		F			133±11.5			Currey, 1976
	Pinctada margaritifera	SN			419±18.7			Currey, 1976
	Pinctada maxima	SN		Polished	423	9.6$^{\nabla}$		Taylor and Layman, 1972
				Dry	382±20	8.5		Taylor and Layman, 1972
		CP		Dry	236±10	8.1$^{\nabla}$		Taylor and Layman, 1972
	Pinctada sp.	SN			332±40.8			Currey, 1976
	Pinna muricata	P			210±32.5			Currey, 1976
	Saccostrea cucullata	CoF			74±10.0			Currey, 1976
	Saxidomus purpuratus	CL	Parallel	Dry	101.6-101.8		W	Yang et al., 2011a
				Wet	109.8-148.0		W	Yang et al., 2011a
			Perpendicular	Dry	105.0		W	Yang et al., 2011a
				Wet	58.8		W	Yang et al., 2011a
	Tridacna gigas	CL	Perpendicular		123			Lin et al., 2006
			Parallel		87			Lin et al., 2006
			Perpendicular		202		D/W	Lin et al., 2006
			Parallel		154		D/W	Lin et al., 2006
	Tridacna maxima	CCL		Wet	213	6.5$^{\nabla}$		Taylor and Layman, 1972
				Dry	244±50	7.6$^{\nabla}$		Taylor and Layman, 1972
		CL		Wet	109	4.4		Taylor and Layman, 1972
				Dry	145±10	7.6$^{\nabla}$		Taylor and Layman, 1972

(*continued on next page*)

by gold/chromium coating. All specimens were observed in the dry condition.

3. Results and discussion

3.1. *Characterization of structure*

Biological materials usually exhibit a hierarchical structure (Baer et al., 1992; Heuer et al., 1992). Currey and Taylor (1974) classified the microstructures of the shells into nacre (columnar and sheet), foliated, prismatic, crossed lamellar, and complex crossed lamellar. Kobayashi and Samata (2006) expanded this classification, identifying more than ten morphological types of bivalve shell structures. They used the names simple prismatic, nacreous, foliated, composite prismatic, crossed lamellar structures, among others to describe them. It should be noted that there is a significant variation in this classification. Often, researchers classify the structures into different names according to their own interpretations.

Visual observation of the cross section of *S. purpuratus* shell reveals three regions: the inside, purple; the middle,

Table 2 (*continued*)

Class	Name	Structure	Test orientation	Treatment	Strength (MPa)	*E* (GPa)	Note	Reference
Gastropods	*Conus betulina* Linnaeus	CL	Plane		240–286			Liang et al., 2008
			Transverse		125–145			Liang et al., 2008
	Conus leopardus	CL			297±22.7			Currey, 1976
	Conus miles	CL			278±7.8			Currey, 1976
	Conus litteratus	CL			301±65.4			Currey, 1976
	Conus prometheus	CL			271±40.9			Currey, 1976
	Conus striatus	CL			336±27.3			Currey, 1976
	Conus virgo	CL			323±60.1			Currey, 1976
	Cypraea tigris	CL			208±18.0			Currey, 1976
	Haliotis rufescens	P(outer)	Perpendicular		540		W	Menig et al., 2000
			Parallel		235		W	Menig et al., 2000
		N(inner)	Perpendicular		735		D/W	Menig et al., 2000
			Parallel		548		D/W	Menig et al., 2000
	Lambis lambis	CL			217±32.8			Currey, 1976
	Patella Mexicana	CF			208±18.8			Currey, 1976
	Patella vulgate	CF			196±30.3			Currey, 1976
	Strombus costatus	CL			280±31.7			Currey, 1976
	Strombus gigas	CL			198±24.8			Currey, 1976
			Perpendicular		166		W	Menig et al., 2001
			Parallel		218		W	Menig et al., 2001
			Perpendicular		249		D/W	Menig et al., 2001
			Parallel		361		D/W	Menig et al., 2001
			Perpendicular		180–210			Menig et al., 2001
			Parallel		210–310			Menig et al., 2001
			Perpendicular		230–300			Menig et al., 2001
			Parallel		320–410			Menig et al., 2001
	Trochus niloticus	CN			320±23.9			Currey, 1976
	Turbo marmoratus	CN			353±18.8			Currey, 1976

N: nacreous, H: homogeneous, CMP: composite prisms, F: foliated, CCL: complex cross-lamellar, CL: cross-lamellar, CP: calcite prisms, SN: sheet nacre, LN: lenticular nacre, P: prismatic, CoF: complex foliated.
Data with $^{\nabla}$ are corrected values. The error in this table is standard deviation.
[W] in notes means data are obtained with Weibull method; [D] in notes means data are obtained from dynamic tests; *E*: modulus.

with a purplish coloration; the outside, white. Fig. 2 shows the overall view of section of the shell in the center. Peripheral drawings and SEM micrographs show the structural characterizations of layers. Similar to the structure of the shell observed by optical microscopy (Yang et al., 2011a,b), the curving lines shown in the cross section indicate the growth course of the shell. In order to distinguish the different structures of the layers, the structural observations of four regions (Regions A, B, C and D) on the cross section of the shell from the outer layer to inner layer are given in detail. All the pictures were taken with the polished or fractured surfaces of the deproteinized specimens using sodium hypochlorite. This deproteinization procedure removed some of the organic interlayer. The outer layer shows a porous structure with nanometer sized particulates around 90–160 nm. The particles are fused together, forming a fibrous/blocky structure in the outer layer close to middle layer. The smooth surfaces of the fiber/block boundary are shown in the picture. When it comes closer to the middle layer, the structure begins to have lamellae.

Both the middle and inner layers show the crossed lamellar structure. The picture in Region C observed on polished specimen shows the boundaries of the lamellae and the pores and particles in the lamellae clearly. These are denoted “areas of granular appearance” by Kennedy et al. (1969) in their description of the complex crossed lamellar structure. The inner layer shows a dense crossed lamellar structure. The unit (lamella) in the crossed lamellar structure is a second-order lamella. Fig. 3(a) shows the statistical distribution of the lamellar thickness obtained by measuring approximately 200 lamellae. The thickness of the majority of lamellae is around 200–600 nm with the highest incidence between 300 and 400 nm. Lamellae oriented in an identical direction form a domain which is called ‘block’ by Kennedy et al. (1969). Such a domain is shown in Fig. 4(a), highlighted by dashed lines. The width of the domains varies much; most of the domains have a width of 10–70 μm as shown in Fig. 3(b). The width of the domains in the middle layer appears larger than that in the inner layer (Yang et al., 2011b). The density of the units in the structure (particles in the outer layer and lamellae in the inner and middle layers) increases gradually from the outer to inner layer.

SEM observations are shown in Fig. 4. Domains with different widths are seen in Fig. 4(a); the boundaries between several domains are highlighted. The crossed lamellae have a chevron appearance. Fig. 4(b) shows another region in which the width of domains (chevron pattern) varies. Due to different specimen preparation, the domains in Fig. 4(a) and (b) look different. The lamellae which comprise the domain are shown in Fig. 4(c). The mean thickness of lamellae is about

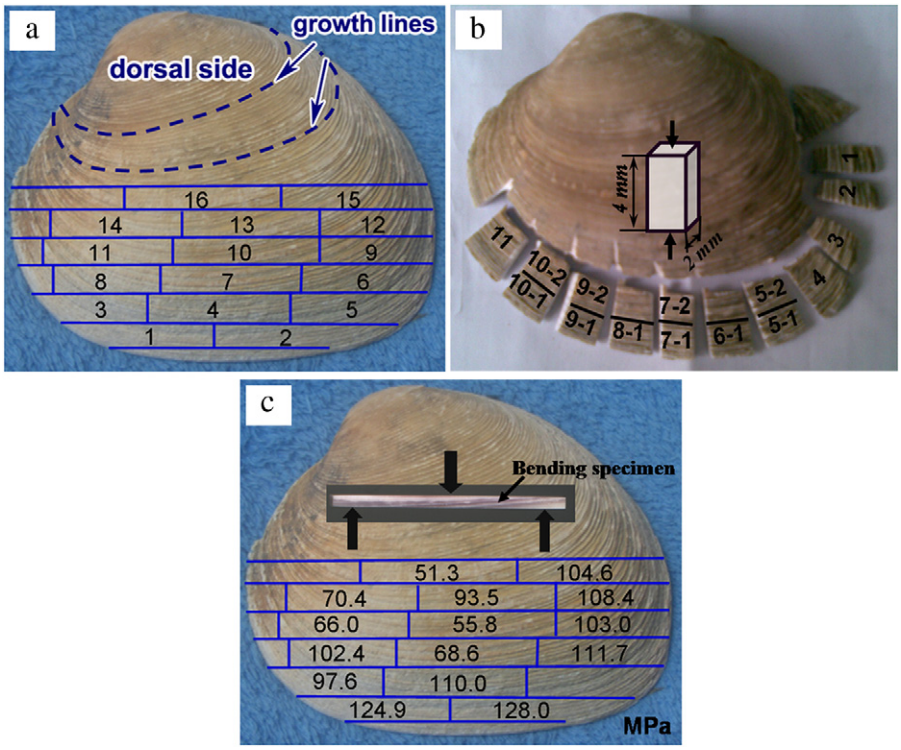

Fig. 1 – Specimens of *Saxidomus* shell showing the dorsal part: (a) orientations of flexure specimens, (b) orientations of compression specimens, and (c) flexure strengths (in MPa) of the specimens distributed in the shell and a bending specimen.

355 nm (consistent with Fig. 3(a)). Organic interlayer materials highlighted by circles can be observed between lamellae in the magnified picture in Fig. 4(d). The organic layer of nacre is known to play a role in enhancing toughness (Meyers et al., 2008).

Fig. 5 shows the detailed morphology of the 'white' outer layer. Fig. 5(a) shows a low magnification of the entire region with a photograph on the right-hand side (above it). The picture on the right is not the one observed by SEM, but is also a general specimen which was taken from the shell lip not far from the dorsal part. There, the growth lines pointed out by the dashed lines are shown on the cross section of the shell alternating purple and purplish layers. The ridges correspond to growth lines on the surface of the shell and the purplish layers are curved at the edge of the shell. Fig. 5(b) and (c) show higher magnifications of the fibrous/blocky structure. The porosity is evident in Fig. 5(d). It is interesting to note that no organic phase was observed.

The crossed lamellar structure in the interior of the shell is characterized by irregular lamellae. Fig. 6(a) shows the irregular shapes of lamellae with thickness varying between 200 and 600 nm. Fig. 6(b) shows the detailed view corresponding to the junction of lamellae. There are spaces left by the irregular thickness, additional or missing lamellae, so some lamellae have to curve to fill the space to ensure contact. For example, in Fig. 6(b), the two full adjacent lines show the lamellae thickness varying along their length; dashed lines show the curving lamellae. Fig. 6(c) shows the intersection of two crossed lamellar domains. When two orientations of lamellae encounter each other, the lamellae are fragmented to form subsections shown in Fig. 6(d). The subsections are less than 1 μm long.

Over 150 measurements of the apparent angles between the lamellae were made. Two of these projected (observed) β_{proj} angles are shown in Figs. 4(b) and 6(c). 85% of the measurements give values β_{proj} larger than 90°. The projected angle is higher than the real angle (see Appendix). Thus, these measurements are consistent with an angle of 90° between lamellae observed.

The cross section of the shell was characterized by SEM after deproteinization in order to reveal the lamellae more clearly. Fig. 7(a), (b) show the inner and middle layers, respectively. Two important observations can be made. Firstly, the lamellae are quite irregular, in contrast with lamellae in *Conus* (Liang et al., 2008) and *Strombus* (Kamat et al., 2000). This is consistent with the thickness measurements in Fig. 3(a). Secondly, the lamella thickness increases from the inner to the middle layer. This can be seen by comparing Fig. 7(a) and (b). Representative thicknesses are marked t_1 and t_2. There is less organic interlayer in the middle layer because the lamellae are thicker; one can also see mineral ligaments (circled) between adjacent lamellae. The detailed nature of the lamellar nanostructure will require characterization by transmission electron microscopy.

3.2. *Mechanical properties*

Because the two valves of the bivalve shell are symmetrical to each other, the distribution of strength in a shell is a better comparison than that of specimens in the same locations

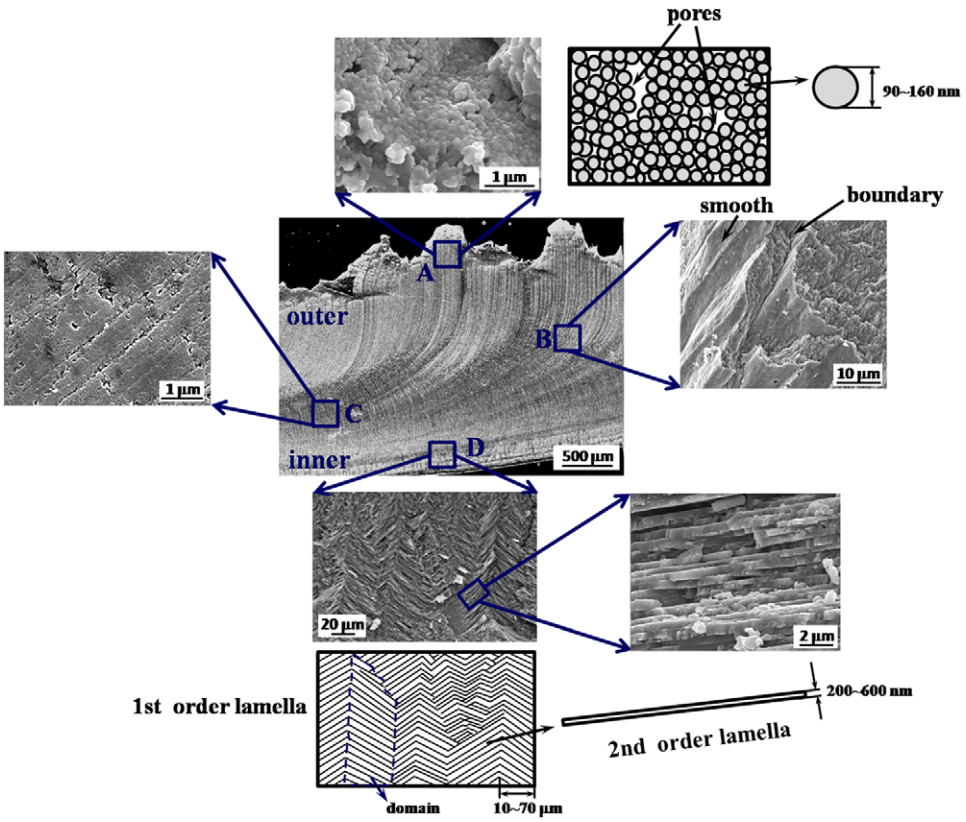

Fig. 2 – Overall view (center) of section of shell showing different morphologies in inner layer (bottom), middle layer (left) and outer regions (top and right).

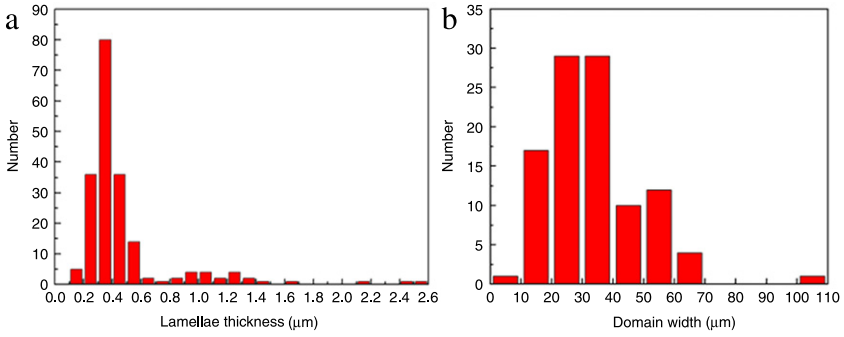

Fig. 3 – Statistical distribution of (a) lamella thickness and (b) domain width.

from different shells. The bending tests were performed with about 20 dry and 15 wet specimens taken from two valves of the same shell to establish this effect. This procedure ensures that the effect of different growth conditions of the shells on mechanical properties is completely eliminated.

The bending strengths of the specimens were measured and analyzed by means of the Weibull equation (Weibull, 1951):

$$P(V) = \exp\left[-\left(\frac{\sigma}{\sigma_0}\right)^m\right] \quad (1)$$

where m is the Weibull parameter modulus and σ_0 is the characteristic stress (not the mean stress). The Weibull modulus, which depends on the distribution of the flaw sizes (Jayatilaka and Trustrum, 1977; Danzer, 1992), is a measure of the variability of strength. The higher the value of m, the less is the variability of the material strength (Meyers and Chawla, 1999). The experimental points are shown in Fig. 8 together with the Weibull curves. The mean stress at probability of 50% [$P(V) = 0.5$] is reached at 93 MPa in bending and m is equal to 3.52 (Fig. 8(a)). In order to further analyze the statistical differences between the dry and wet conditions, specimens were extracted from four dry and two wet shells and subjected to three-point bending tests. The Weibull plots for dry and wet conditions are shown in Fig. 8(b). The strength of dry specimens is less variable (higher Weibull modulus) than that of wet specimens. This might be due to the mineral

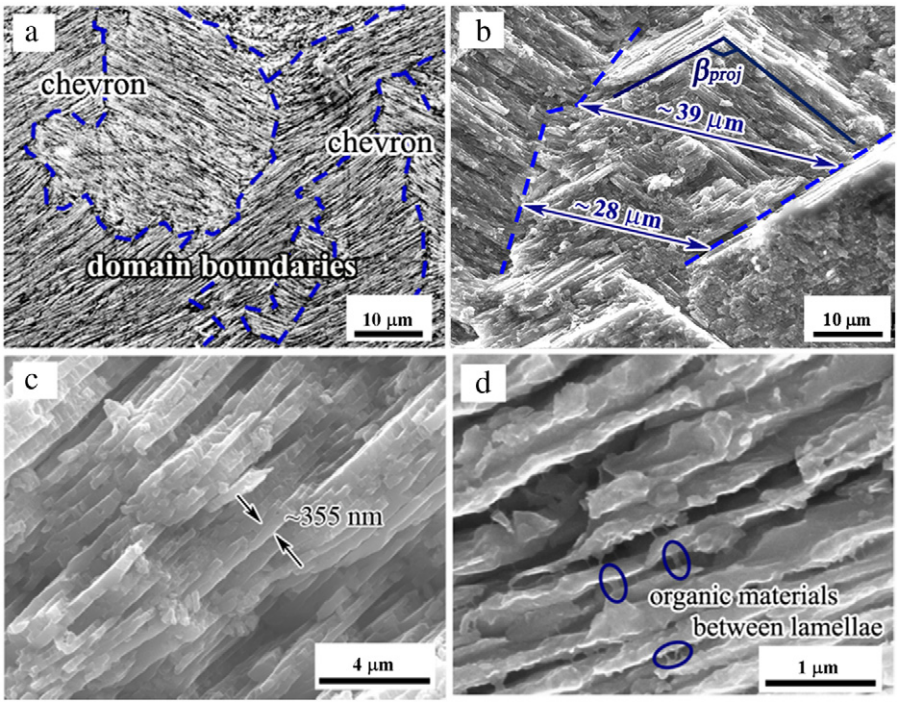

Fig. 4 – Characteristic structure of *Saxidomus purpuratus*: (a) irregular domain boundaries, (b) chevron pattern of domains, (c) parallel lamellae, and (d) lamellae that underwent separation showing organic intertile layer stretched (circled).

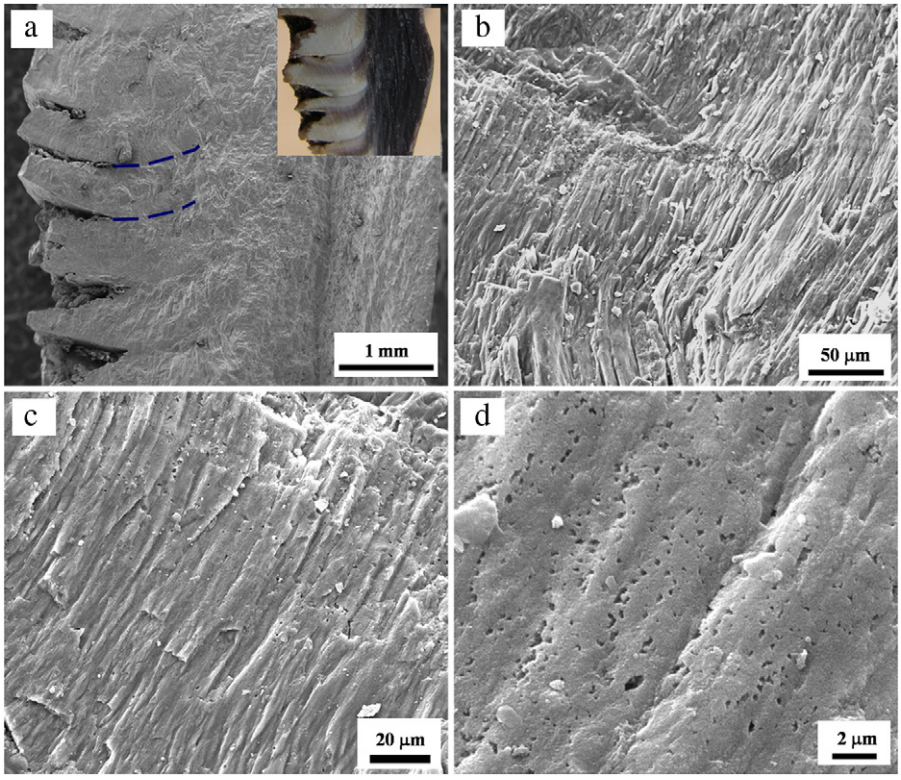

Fig. 5 – Views of outer layer of the shell: (a) a low magnification SEM micrograph showing growth ridges with a photograph representing entire cross section on the right-hand side, (b) the fibrous/blocky structure of the outer layer, (c) a higher magnification of the blocky structure, and (d) porosity in the structure.

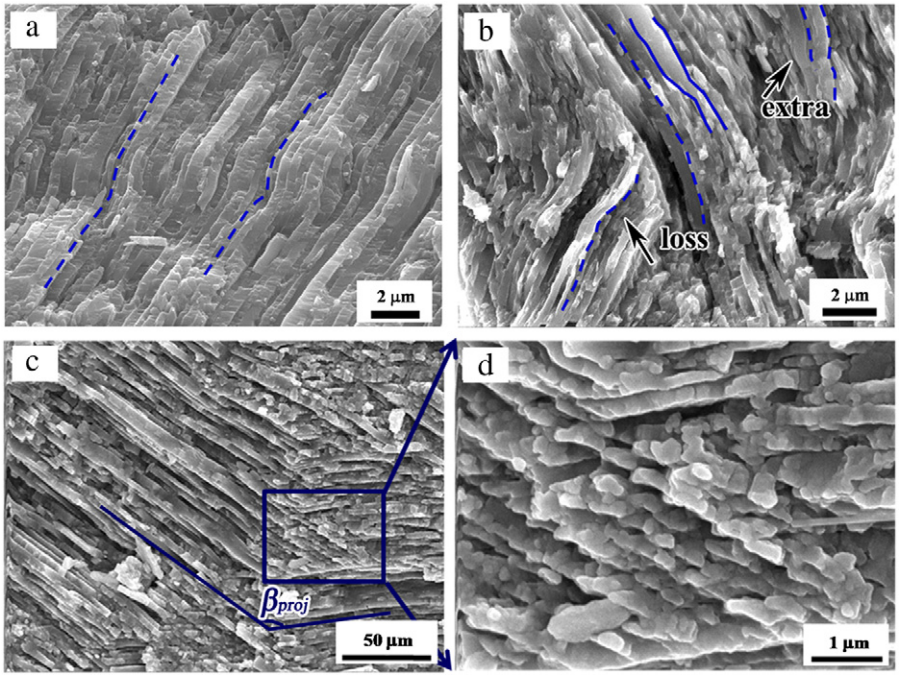

Fig. 6 – Characteristics of the lamellae in structure: (a) irregular shapes of lamellae, (b) curved lamellae, (c) the intersection of the crossed lamellae, and (d) subsections in the intersection.

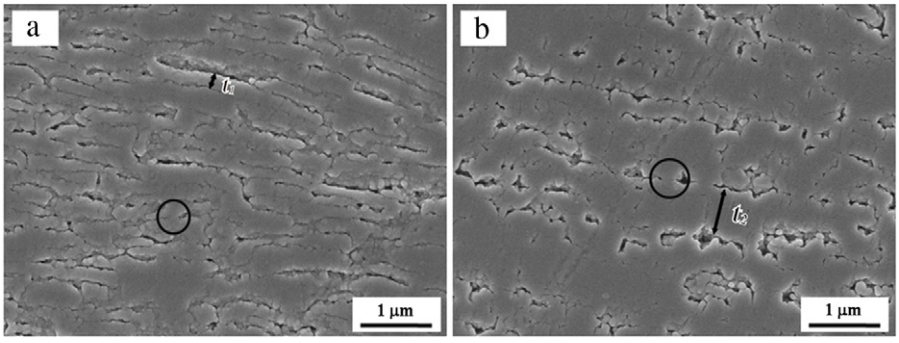

Fig. 7 – Polished and deproteinized sections at (a) inner and (b) middle layers; note irregular lamellae shapes and smaller thickness in inner layer. Mineral bridges (ligaments) marked by circles. Lamella thickness marked by t_1 (inner layer) and t_2 (middle layer).

layers playing a more prominent role due to the dehydration of the organic materials.

Two shells were subjected to three-point bending tests. One valve of the shell was tested in the dry condition and the other valve in the wet. The Weibull plots for two pairs of shells are shown in Fig. 8(c) and (d). There is no significant difference between dry and wet conditions in each valve but Shell I and Shell II (different pairs) show results that are quite different. This shows that there is a significant variation in Weibull strength (from 82–88 MPa to 102–104 MPa) between different shells. The mean tensile (flexure) strength at probability of 50%, 80–105 MPa, is on the same order as the compressive strength (~ 50–150 MPa) obtained by Yang et al. (2011a) and the Weibull moduli vary from 3.0 to 7.6. Hence, the compressive and flexure strengths are, compared to the strongest shells (Tables 1 and 2) fairly low. Possible reasons for this are a low fraction of organic interlayer and porosity in the outer layer.

Hardness tests were performed on the cross section of the shell to establish whether there is variation of the strength correlating with the colors of the layers; the results are shown in Fig. 9. It is easy to distinguish the purple and white regions from the hardness results. The hardness of the purple region is about 2500 MPa while that of the white region is about 1750 MPa. Compared with the white and purple regions, the hardness of the purplish area varies more. The typical morphologies of indentations in purple and white region are shown in Fig. 10. Fig. 10(a) shows the white region with curving lines on it. These lines are marked by arrows in the picture and are due to growth effects that could be seasonal. These lines are also evident in Fig. 2. Fig. 10(b) and (c) show the indentations in the white and purple regions, respectively. Cracks in the white region may propagate continuously by

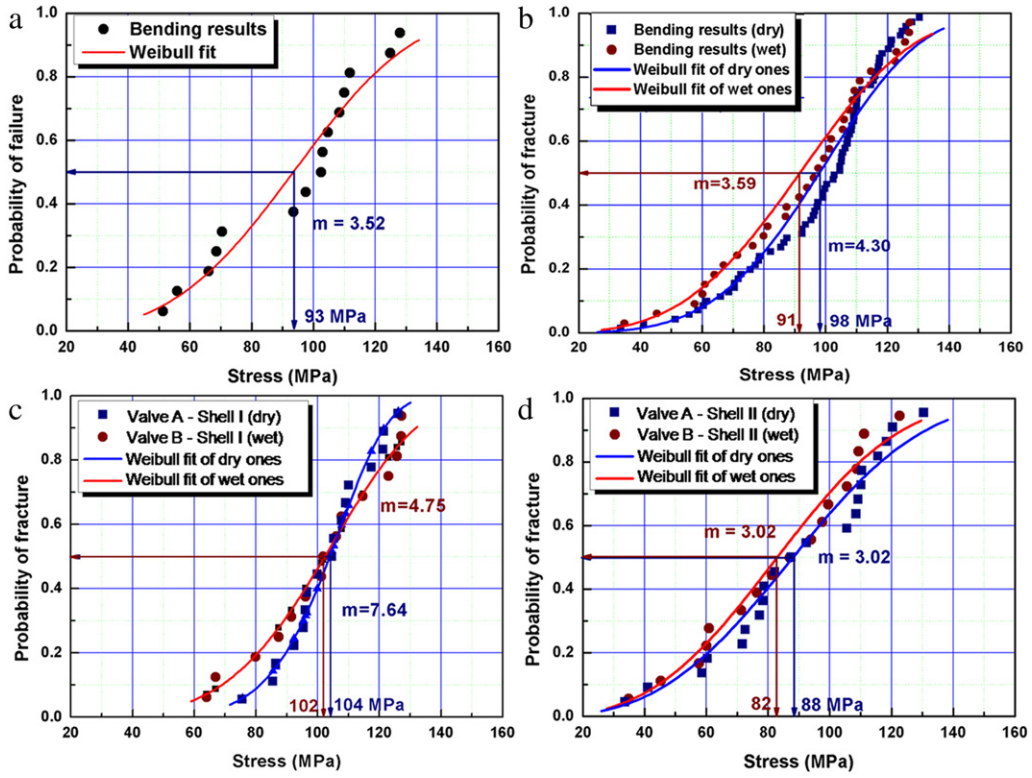

Fig. 8 – Weibull plots of bending strengths from different shells: (a) bending strengths of the shell shown in Fig. 1(a), (b) bending strengths of all dry and wet specimens, (c) bending strengths of dry and wet specimens from two valves of a shell, and (d) bending strengths of dry and wet specimens from two valves of another shell.

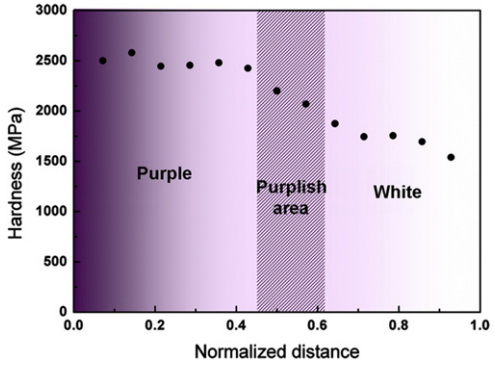

Fig. 9 – Vickers microhardness along the cross section of shell as a function of distance from inside; each point represents the average of three readings.

encountering the pores. Hence, the damage ahead of the indentation in the white region with a porous fibrous/blocky structure is more serious than in the purple region. Under the same load, the size of the crack in the purple region is smaller than in the white region, which is indicative of a greater toughness (Evans and Charles, 1976).

Fig. 11 shows the details of an indentation in the purple region with crossed lamellar structure. The crack at one corner of the indent is seen in Fig. 11(a). Fig. 11(b) and (c) show higher magnification views of the crack. Along the extension of the crack, there are some uncracked mineral ligaments which are shown by three arrows in Fig. 11(b). The structure is crossed lamellar and the crack is not continuous; uncracked mineral ligaments form in the purple region. On the other hand, in the white regions the pores provide an easy path for cracks. This mechanism is shown in schematic fashion in Fig. 12. Fig. 12(a) shows the crack produced by the indentation in the inner layer with the crossed lamellar structure. Because of the different orientations of lamellae, the cracks propagate along weak interfaces between lamellae and are then arrested. The cracks are reformed with a gap between them. Thus, uncracked ligaments are formed. Two scenarios are shown: I and II. In Scenario I, a second crack is nucleated in the same lamella; in Scenario II, a second crack is nucleated in a different lamella. Fig. 12(b) shows the mechanism in the outer layer. Cracks produced around the indent can propagate through the pores in the structure. It is clear that the fibrous/blocky porous structure is weaker than the crossed lamellar structure, leading to a greater damage in the former. There are two principal reasons for the lower hardness in the outside region: porosity and the fibrous/blocky structure.

3.3. *Characterization of damage and fracture surfaces*

3.3.1. *Compressive failure*

The compression tests were performed with the specimens shown in Fig. 1(b) with loading direction in the plane of the shells parallel to the surface and perpendicular to the growth lines. Compression curves of the No. 2 and No. 5-1 specimens are shown in Fig. 13. The maximum compressive stresses

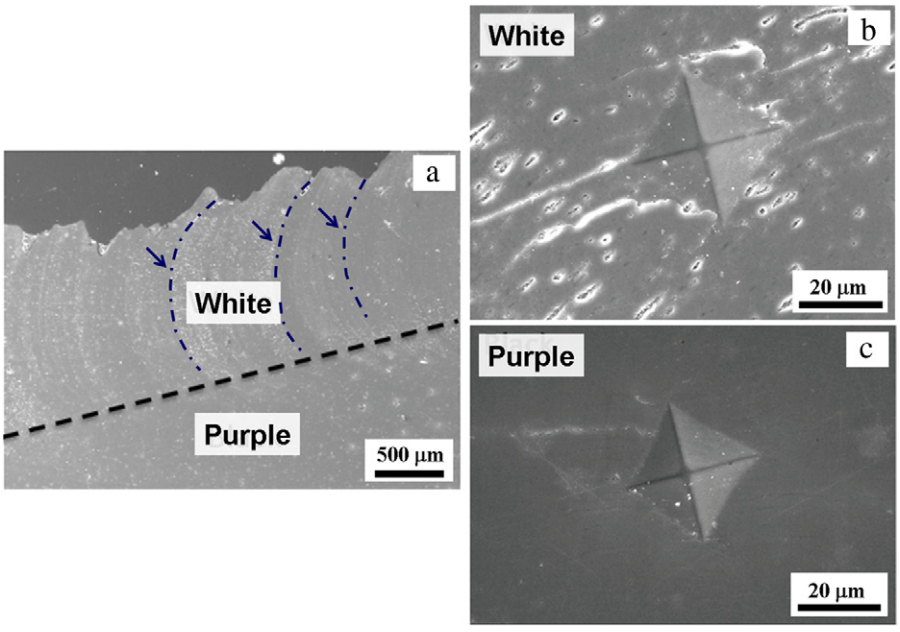

Fig. 10 – Indentations in cross section of shell: (a) white and purple regions with the curving line which are due to growing conditions, (b) indentation in the white region, and (c) indentation in the purple region.

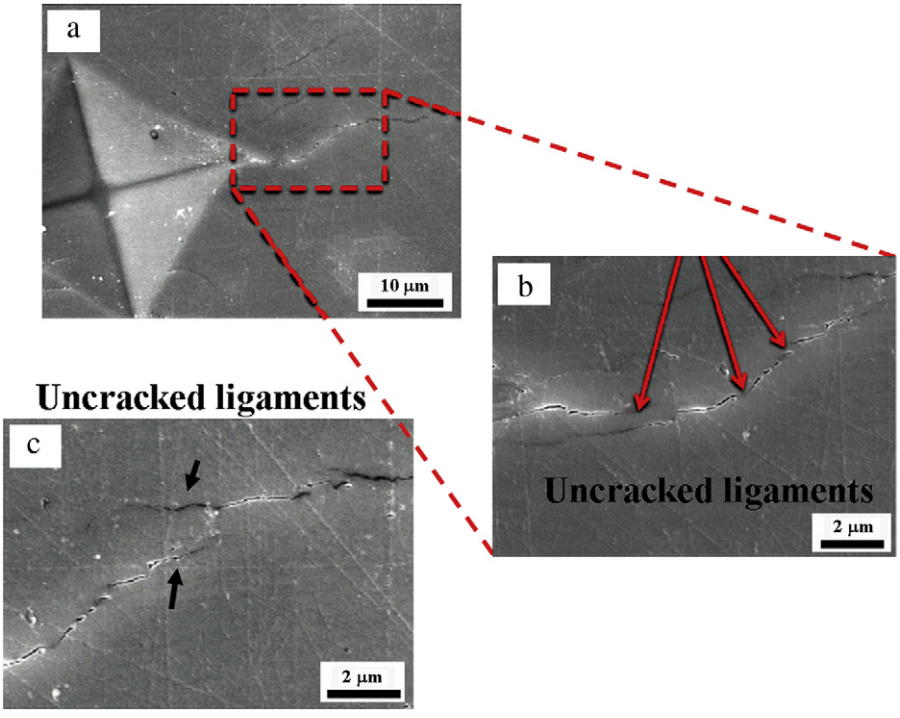

Fig. 11 – Crack emanating from indentation on the inner layer of the cross-sectional specimen: (a) crack near the indentation, and ((b), (c)) the crack morphology at higher magnification.

are 45 MPa and 80 MPa, respectively. Compared with the other results in Table 1, the bending strengths of *S. purpuratus* shells in our research are a little higher than most of the bending strengths of the bivalves. A more detailed account of compression test results is presented by Yang et al. (2011a). Fig. 13 also shows No. 2 and No. 5-1 specimens fractured during the test. Their compression curves can explain the compression fracture path more clearly. These are clearly axial splitting cracks: the compressive stress causes localized tension which opens a crack parallel to the loading direction. There is one platform on the curve of No. 2 specimen and two on the curve of No. 5-1 specimen. The compression

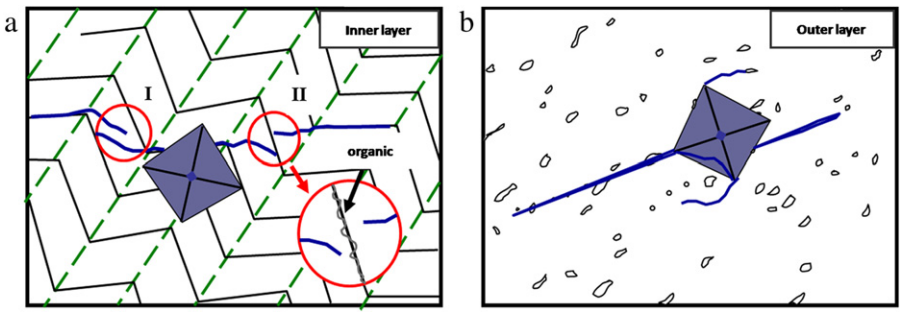

Fig. 12 – Schematic drawing of cracks caused by the indentation in different layers of the shell: (a) inner layer, and (b) outer layer.

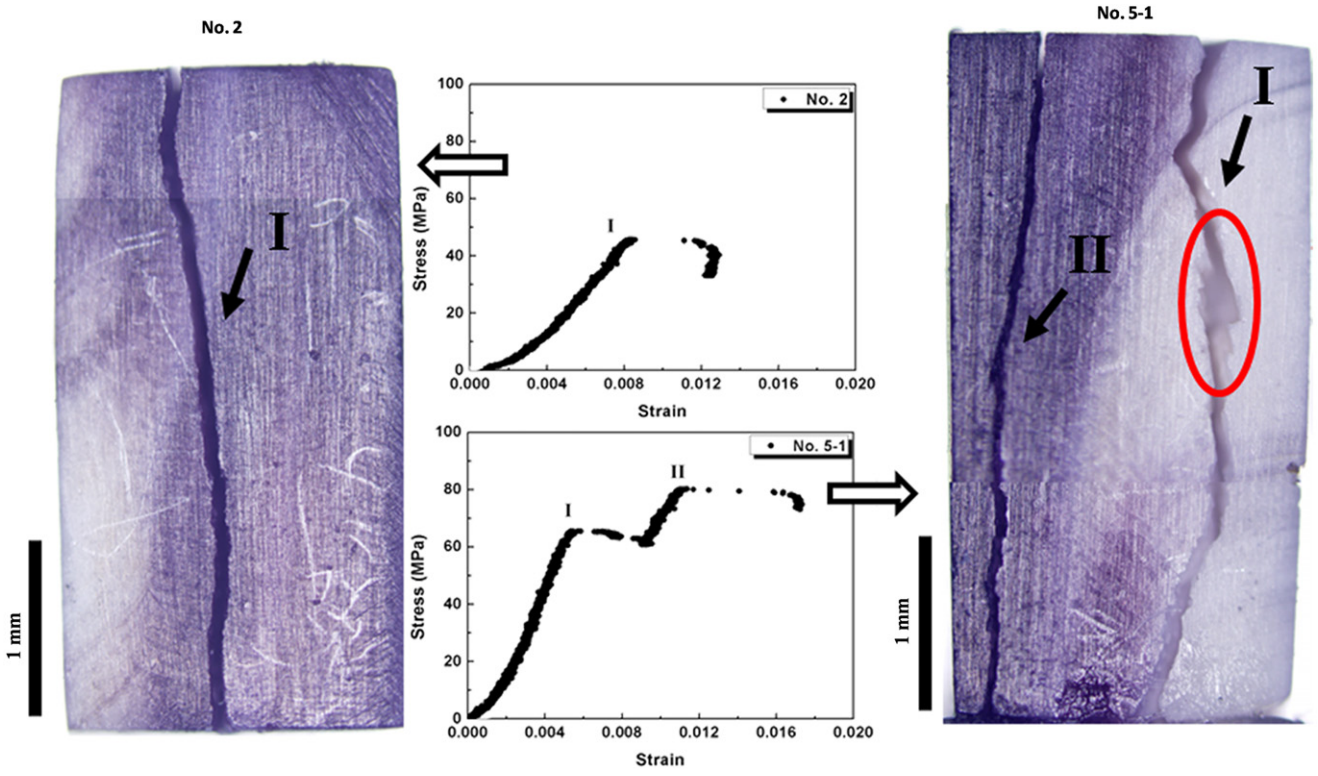

Fig. 13 – Failure of specimen 2# and (5-1)# in compression by axial splitting with their compression curves.

curves can be correlated to the morphology of the specimens after compression tests. Generally, the beginning of each platform corresponds to crack initiation. No. 2 specimen only has one crack and its compression curve has one platform, while No. 5-1 specimen has two cracks in both the external (white) and internal (purple) regions corresponding to two platforms. Crack I with an irregular path is formed first; the strength of the outer layer is lower than that of the inner and the crack is apparently easy to generate. The morphology of the cracking paths supports this; there is a considerable damage and tortuosity in Crack I which also shows evidence of compressive failure (circled), while Crack II is similar to the crack in No. 2 specimen and shows clearly the result of axial splitting.

3.3.2. *Flexure failure: relationship between damage and properties*

Because the inner and middle layers have the same crossed lamellar structure and the hardness of the two layers changes little, specimens were prepared mainly with the inner and middle layers as possible, by removing the outer layer through polishing. However, the shape of the cross section of the shell parallel to the growth lines is curved; hence, some specimens contain the outer layer, especially the ones close to the dorsal part where the curvature is highest. All the bending specimens exhibit a tensile mode of fracture. Both the cracking path and fracture surfaces occurring in bending specimens depend on the arrangement of the lamellae or the domains in the crossed lamellar structure of the shell.

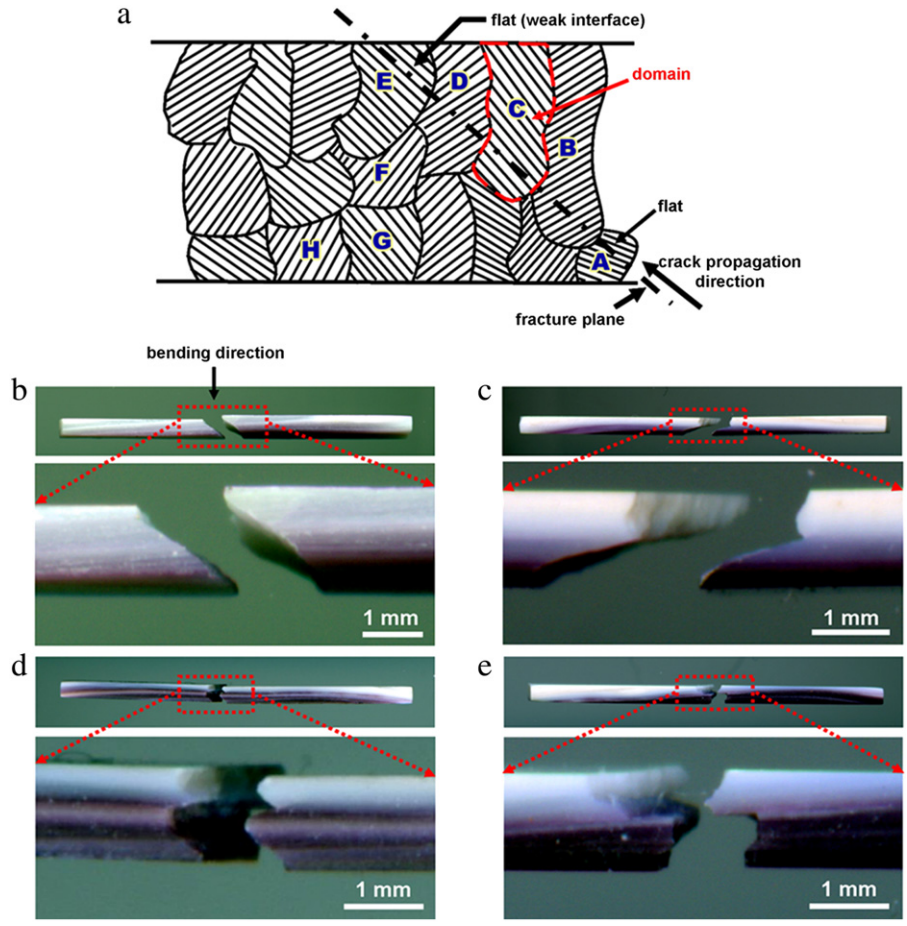

Fig. 14 – Schematic drawing showing how the crack propagates through the structure and typical cracking path morphologies. (a) Schematic drawing of microstructure of shell with crack propagation path alternating by lamella boundary separation (weak interfaces) and lamella fracture, (b) specimen showing an inclined cracking path, (c) specimen showing a cracking path deflected at a large angle corresponding to the color change in the layers, (d) specimen showing a "zigzag" cracking path at one side, and (e) similar to the specimen in (d) showing a large step at the other side.

Fig. 14(a) shows a schematic drawing of the cracking path in the microstructure. The actual cracking paths in specimens No. 2, No. 11, No. 16 are shown in Fig. 14(b–e). In Fig. 14(a) the crack starts at the right-hand bottom side, progresses by going through alternating flat, hatched, flat, hatched regions. Neighboring domains are oriented at specific angles and thus the structure forms a crossed lamellar pattern. This crack, marked by a dashed line in Fig. 14(a), follows the path A, B, C, D, E.

Thus, the fracture path in the actual specimens is determined by the orientation of the domains. When the crack goes through a domain, it travels preferentially along the interfaces between lamellae. These may change the direction of the crack and extend the cracking path. Fig. 14(b) shows the cracking path of specimen No. 2 in Fig. 1(a). The cracking path is almost an inclined fracture. This suggests that the crack goes though one direction of the lamellae more than the other. Shown in the schematic drawing in Fig. 14(a), the crack would propagate by going though Regions H, F and D. This kind of structure can lengthen the path of the crack and cause more energy to be absorbed in the fracture process.

Fig. 14(c) shows the cracking path of specimen No. 11. The cracking path exhibits a clear change in orientation. The crack first goes in an inclined way like the cracking path of No.2 specimen and then goes in "zigzag" path shown as through Regions G, F and E in Fig. 14(a). Seeing the morphology of the cracking path, the color of the cross section of the specimen changes a little more conspicuously. Between the white and purple regions, the crack tends to deflect at a large angle. In the schematic drawing of Fig. 14(a), the crack propagates though Regions H, F and E in sequence. The crack goes through several domains with the same orientation of lamellae and then through some with different orientations of lamellae. The cracking path of No. 16 specimen observed from both sides is shown in Fig. 14(d) and (e). It is a complex cracking path which is not symmetrical in the two cross sections of a same specimen due to the deflection of the crack at a large angle between the white and purple regions.

Fig. 15 shows the fracture surfaces of the purple region parallel to the external shell lip. Two features are seen clearly in Fig. 15(a): flat regions and hatched (irregular) regions. The flat and hatched regions may be formed as cracks go through the interfaces and cross sections of the second-order

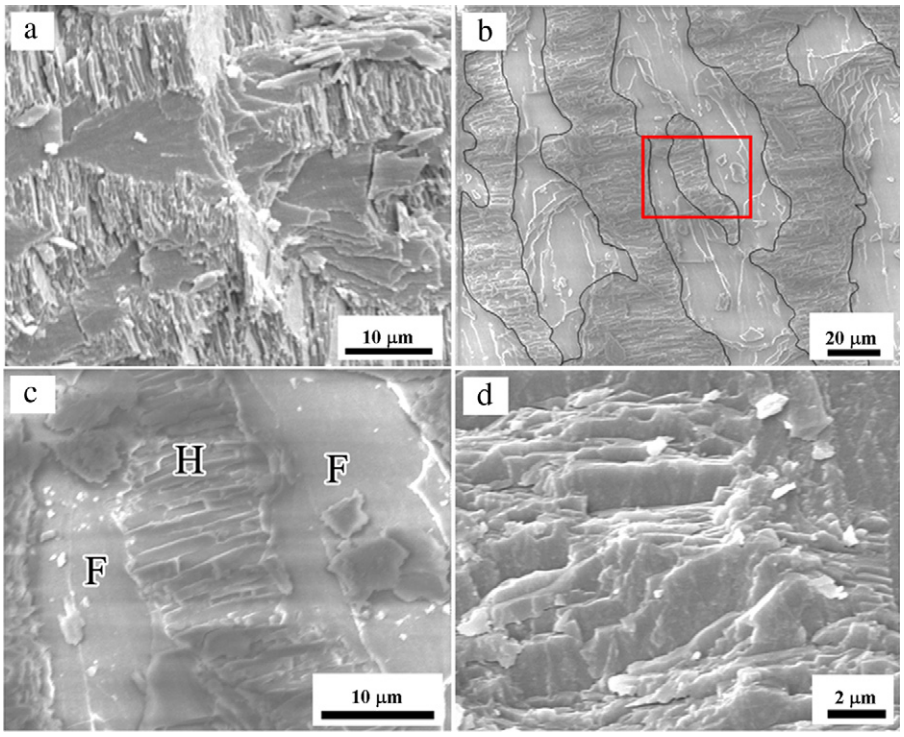

Fig. 15 – Appearance of fracture surface in the purple region: (a) SEM micrograph showing alternating flat and hatched regions, (b) tracing of fracture domains, (c) central region showing crack perpendicular to lamellae (H) and sides showing crack parallel to lamellae (F), and (d) crack at an angle to lamellae showing a sequence of intertile fractures and fractures perpendicular to lamellae.

lamellae, respectively. It can be imagined that if the cracking path is from the bottom to the top, the crack propagated from the hatched region, flat region, hatched region and so on, like the cracking path in Fig. 14(a) through B, C, D and E. The domains are delineated in Fig. 15(b) to show the two areas clearly. The boundaries between these two domains are irregular and they are approximately 10–70 μm wide as shown in Fig. 2. A closer observation of the hatched regions, Fig. 15(c), shows that they are composed of parallel lines delimiting the boundaries of lamellae. The thickness of these layers in Fig. 15(c) is less than 1 μm. This is not the real lamella thickness, since the fracture plane is not necessarily perpendicular to the lamella plane. In Fig. 4(c), these lamellae are shown in a clearer fashion, and their thickness is ~0.35 μm. Thus, the crossed lamellar structure provides excellent barriers for crack propagation since the crack will always encounter lamellae that need to be fractured along its path.

It is clear from the observations that the fracture does not follow the planes perpendicular to the maximum tensile normal stresses. Rather, the fracture surfaces are at an angle. This can be explained by observing the fracture surfaces. The interfaces between lamellae are weak. Thus, the crack favors these planes, which correspond to the flat areas in Fig. 15. However, to cross from one flat area to the next, the cracks have to traverse the 'hatched region'. This requires fracturing of the individual lamellae, and this is seen in the detailed micrograph of Fig. 15(d).

4. Summary and conclusions

The strength and fracture behavior of *S. purpuratus* shells were investigated systematically and correlated with their structures. The following conclusions can be drawn:

1. The shell has three layers, inner, middle and outer. The outer layer shows a porous and fibrous/blocky structure containing nanosized particles. The structures of the inner and middle layers are crossed lamellar with domains of parallel lamellae at different orientations. The width of the domains (10–70 μm) increases from inner to middle layers. The thickness of the lamellae in the domains ranges between 200 and 600 nm. A statistical measurement shows that the highest incidence is between 300 and 400 nm. The density of the lamellae and the compactness and homogeneity of their structure decreases gradually from the inner to the outer layer.
2. The principal difference between the inside and outside layers is the structure which can contribute to the cracking path. This reflects itself in a decrease in microhardness. The cracks in the inner layer may stop when encountering at an identical lamella or the organic interlayer, while the cracks may be easier to propagate in the outer layer as the pores provide an easy path.
3. The three-point flexure strengths of dry and wet specimens were determined and analyzed by Weibull statistics. The strength of dry specimens is a little higher than the strength of the wet ones.

4. Two valves of the bivalve shell were tested in the wet and dry conditions, revealing that the differences from shell to shell (102–104 MPa vs. 82–88 MPa) are much more significant than the effect of hydration within one shell. The average flexure strength of the shells is 98 MPa in the dry condition and 91 MPa in the wet condition.
5. The compressive strength of *Saxidomus* shell (50–150 MPa; Yang et al., 2011a) is, compared to other shells (Table 2) fairly low. Possible reasons for this are a low fraction of organic interlayer and porosity in the outer layer. The compression path can be correlated to the formation of the cracks by compression and axial splitting.
6. The flexure and compressive strengths of the *Saxidomus* shells are of the same order; this is directly linked to the toughness of the shell.
7. Cracks propagate preferentially along the interfaces between lamellae. The cracking path depends on the orientations of the lamellae in the domains traversed by the cracks. The crack tends to deflect at a large angle between the white and purple regions in the cross section of the specimens. This creates a complex cracking path which is not symmetrical in the two cross sections of a same specimen.
8. The results are consistent with an anisotropic hierarchical structure of the *Saxidomus* shell and with previous studies on other shells.

Acknowledgments

This work was supported by the National Natural Science Foundation of China (Grant No. 50890173), the National Basic Research Program of China (Grant No. 2010CB631003), the Fundamental Research Funds for the Central Universities of China (Grant No. N090505001) and the Program for New Century Excellent Talents in University, Ministry of Education, PR China (NCET-07-0162). We would like to thank Chung-Ting Wei who helped us with hardness tests and some SEM observations.

Appendix. Calculation of projected angle

Let a general angle β be projected on a plane (observation plane). The relationship between the real angle β and its projection on the observation plane $\alpha_{obs}(\alpha_{proj})$ is derived below. Fig. A.1 shows the schematic of planes. The two orientations AB and AC define a plane α. We assume that they are symmetrical with respect to the projection plane. α and α_{proj} (α_{obs}) intersect along BC. From trigonometric relations in the triangles ABC and BCD, we can obtain the relationship between the angles β and β_{proj}.

Let us draw perpendiculars to the intersection BC passing through A and D. These are segments EA and ED.

ΔABE:

$$\tan\frac{\beta}{2}=\frac{BE}{AE}. \tag{A.1}$$

ΔBDE:

$$\tan\frac{\beta_{proj}}{2}=\frac{BE}{ED}. \tag{A.2}$$

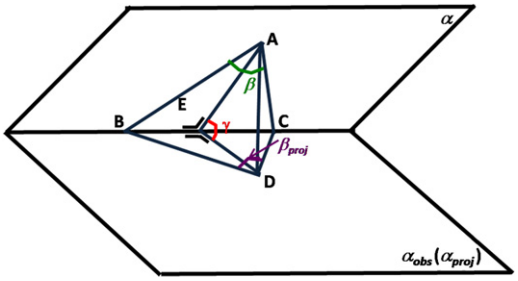

Fig. A.1 – Schematic of real angle β between lamellae (plane α) and observation plane (plane α_{obs}) with projected angles β_{proj} between lamellae.

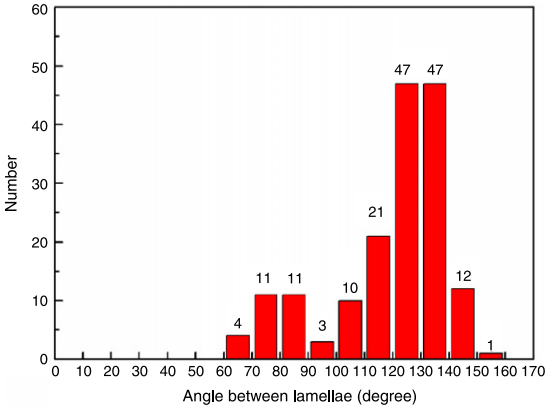

Fig. A.2 – Distribution of the observed angles between lamellae; number of measurements marked on top of each column.

ΔAED:

$$\cos\gamma=\frac{ED}{AE}. \tag{A.3}$$

From (A.1) and (A.2),

$$\frac{\tan\beta/2}{\tan\beta_{proj}/2}=\frac{ED}{AE}.$$

From (A.3):

$$\frac{\tan\beta/2}{\tan\beta_{proj}/2}=\cos\gamma.$$

So,

$$\tan\frac{\beta_{proj}}{2}=\cos\gamma\cdot\tan\frac{\beta}{2}.$$

Fig. A.2 shows the measurements of the projected angles β_{proj}. 169 measurements were made, of which 85% give a value larger than 90°.

Hence, the measurements are consistent with 90° orientation between adjacent lamella domains. This analysis does not apply to observations of apparent angles on a flat (polished) surface.

REFERENCES

Baer, E., Hiltner, A., Morgan, R.J., 1992. Biological and synthetic hierarchical composites. Phys. Today 45, 60–67.

Barthelat, F., Li, C.M., Comi, C., Espinosa, H.D., 2006. Mechanical properties of nacre constituents and their impact on mechanical performance. J. Mater. Res. 21, 1977–1986.

Barthelat, F., Tang, H., Zavattieri, P.D., Li, C.M., Espinosa, H.D., 2007. On the mechanics of mother-of-pearl: a key feature in the material hierarchical structure. J. Mech. Phys. Solids 55, 306–337.

Checa, A.G., Rodríguez-Navarro, A.B., 2005. Self-organisation of nacre in the shells of Pterioida (Bivalvia: Mollusca). Biomaterials 26, 1071–1079.

Checa, A.G., Rodríguez-Navarro, A.B., Esteban-Delgado, F.J., 2005. The nature and formation of calcitic columnar prismatic shell layers in pteriomorphian bivalves. Biomaterials 26, 6404–6414.

Chen, P.Y., Lin, A.Y.M., Lin, Y.S., Seki, Y., Stokes, A.G., Peyras, J., Olevsky, E.A., Meyers, M.A., McKittrick, J., 2008. Structure and mechanical properties of selected biological materials. J. Mech. Behav. Biomed. Mater. 1, 208–226.

Currey, J.D., 1977. Mechanical properties of mother of pearl in tension. Proc. R. Soc. Lond. B 196, 443–463.

Currey, J.D., 1976. Further studies on the mechanical properties of mollusc shell material. J. Zool. Lond. 180, 445–453.

Currey, J.D., Kohn, A.J., 1976. Fracture in the cross-lamellar structure of Conus shells. J. Mater. Sci. 11, 1615–1623.

Currey, J.D., Taylor, J.D., 1974. The mechanical behavior of some molluscan hard tissues. J. Zool. Lond. 173, 395–406.

Danzer, R., 1992. A general strength distribution function for brittle materials. J. Eur. Ceram. Soc. 10, 461–472.

Evans, A.G., Charles, E.A., 1976. Fracture toughness determinations by indentation. J. Am. Ceram. Soc. 59, 371–372.

Evans, A.G., Suo, Z., Wang, R.Z., Aksay, I.A., He, M.Y., Hutchinson, J.W., 2001. Model for the robust mechanical behavior of nacre. J. Mater. Res. 16, 2475–2484.

Gao, H.J., Ji, B.H., Jäger, I.L., Arzt, E., Fratzl, P., 2003. Materials become insensitive to flaws at nanoscale: lessons from nature. Proc. Nati. Acad. Sci. USA 100, 5597–5600.

Heuer, A.H., Fink, D.J., Laraia, V.J., Arias, J.L., Calvert, P.D., Kendall, K., Messing, G.L., Blackwell, J., Rieke, P.C., Thompson, D.H., Wheeler, A.P., Veis, A., Caplan, A.I., 1992. Innovative materials processing strategies: a biomimetic approach. Science 255, 1098–1105.

Jackson, A.P., Vincent, J.F.V., Turner, R.M., 1988. The mechanical design of nacre. Proc. R. Soc. Lond. B 234, 415–440.

Jayatilaka, A.D.S., Trustrum, K., 1977. Statistical approach to brittle fracture. J. Mater. Sci. 12, 1426–1430.

Ji, B.H., 2008. A study of the interface strength between protein and mineral in biological materials. J. Biomech. 41, 259–266.

Jia, X., Ling, X.M., Tang, D.H., 2006. Microstructures and friction-wear characteristics of bivalve shells. Tribol. Int. 39, 657–662.

Kamat, S., Su, X., Ballarini, R., Heuer, A.H., 2000. Structural basis for the fracture toughness of the shell of the conch Strombus gigas. Nature 405, 1036–1040.

Katti, K.S., Katti, D.R., 2006. Why is nacre so tough and strong? Mater. Sci. Eng. C 26, 1317–1324.

Katti, D.R., Katti, K.S., Sopp, J.M., Sarikaya, M., 2001. 3D finite element modeling of mechanical response in nacre-based hybrid nanocomposites. Comput. Theor. Polym. Sci. 11, 397–404.

Kennedy, W.J., Taylor, J.D., Hall, A., 1969. Environmental and biological controls on bivalve shell mineralogy. Biol. Rev. 44, 499–530.

Kobayashi, I., Samata, T., 2006. Bivalve shell structure and organic matrix. Mater. Sci. Eng. C 26, 692–698.

Kuhn-Spearing, L.T., Kessler, H., Chateau, E., Ballarini, R., Heuer, A.H., Spearing, S.M., 1996. Fracture mechanisms of the Strombus gigas conch shell: implications for the design of brittle laminates. J. Mater. Sci. 31, 6583–6594.

Laraia, V.J., Heuer, A.H., 1989. Novel composite microstructure and mechanical behavior of mollusk shell. J. Am. Ceram. Soc. 72, 2177–2179.

Li, X.D., Xu, Z.H., Wang, R.Z., 2006. In situ observation of nanograin rotation and deformation in nacre. Nano Lett. 6, 2301–2304.

Liang, Y., Zhao, J., Wang, L., Li, F.M., 2008. The relationship between mechanical properties and crossed-lamellar structure of mollusk shell. Mater. Sci. Eng. A 483, 309–312.

Lin, A.Y.M., Chen, P.Y., Meyers, M.A., 2008. The growth of nacre in the abalone shell. Acta Biomater. 4, 131–138.

Lin, A.Y.M., Meyers, M.A., 2005. Growth and structure in abalone shell. Mater. Sci. Eng. A 390, 27–41.

Lin, A.Y.M., Meyers, M.A., Vecchio, K.S., 2006. Mechanical properties and structure of Strombus gigas, Tridacna gigas, and Haliotis rufescens sea shells: a comparative study. Mater. Sci. Eng. C 26, 1380–1389.

Menig, R., Meyers, M.H., Meyers, M.A., Vecchio, K.S., 2000. Quasi-static and dynamic mechanical response of Haliotis rufescens (abalone) shells. Acta Mater. 48, 2383–2398.

Menig, R., Meyers, M.H., Meyers, M.A., Vecchio, K.S., 2001. Quasi-static and dynamic mechanical response of Strombus gigas (conch) shells. Mater. Sci. Eng. A 297, 203–211.

Meyers, M.A., Chawla, K.K., 1999. Mechanical Behavior of Materials. Prentice-Hall, USA.

Meyers, M.A., Lin, A.Y.M., Chen, P.Y., Muyco, J., 2008. Mechanical strength of abalone nacre: role of the soft organic layer. J. Mech. Behav. Biomed. Mater. 1, 76–85.

Nakahara, H., Kakei, M., Bevelander, G., 1982. Electron microscopic and amino acid studies on the outer and inner shell layers of Haliotis rufescens. Venus Jpn. J. Malac. 41, 33–46.

Nukala, P.K.V.V., Simunovic, S., 2005. A continuous damage random thresholds model for simulating the fracture behavior of nacre. Biomaterials 26, 6087–6098.

Sarikaya, M., Aksay, I.A., 1992. Nacre of abalone shell: a natural multifunctional nanolaminated ceramic–polymer composite material. Results Probl. Cell. Differ. 19, 1–26.

Sarikaya, M., Gunnison, K.E., Yasrebi, M., Aksay, I.A., 1990. Mechanical property-microstructural relationships in abalone shell. Mater. Res. Soc. 174, 109–116.

Song, F., Soh, A.K., Bai, Y.L., 2003. Structural and mechanical properties of the organic matrix layers of nacre. Biomaterials 24, 3623–3631.

Su, X.W., Belcher, A.M., Zaremba, C.M., Morse, D.E., Stucky, G.D., Heuer, A.H., 2002. Structural and microstructural characterization of the growth lines and prismatic microarchitecture in red abalone shell and the microstructures of abalone “flat pearls”. Chem. Mater. 14, 3106–3117.

Su, X.W., Zhang, D.M., Heuer, A.H., 2004. Tissue regeneration in the shell of the giant queen conch, Strombus gigas. Chem. Mater. 16, 581–593.

Tang, H., Barthelat, F., Espinosa, H.D., 2007. An elasto-viscoplastic interface model for investigating the constitutive behavior of nacre. J. Mech. Phys. Solids 55, 1410–1438.

Taylor, J.D., Layman, M., 1972. The mechanical properties of bivalve (Mollusca) shell structures. Palaeontology 15, 73–87.

Wang, R.Z., Suo, Z., Evans, A.G., Yao, N., Aksay, I.A., 2001. Deformation mechanisms in nacre. J. Mater. Res. 16, 2485–2493.

Weibull, W., 1951. A statistical distribution function of wide applicability. J. Appl. Mech. 18, 293–297.

Yang, W., Kashani, N., Li, X.W., Zhang, G.P., Meyers, M.A., 2011a. Structural characterization and mechanical behavior of a bivalve shell (*Saxidomus purpuratus*). Mater. Sci. Eng. C 31, 724–729.

Yang, W., Zhang, G.P., Liu, H.S., Li, X.W., 2011b. Microstructural characterization and hardness behavior of a biological *Saxidomus purpuratus* shell. J. Mater. Sci. Technol. 27, 139–146.

Zaremba, C.M., Belcher, A.M., Fritz, M., Li, Y.L., Mann, S., Hansma, P.K., Morse, D.E., Speck, J.S., Stucky, G.D., 1996. Critical transitions in the biofabrication of abalone shells and flat pearls. Chem. Mater. 8, 679–690.